



Ceramic foams directly-coated with flame-made V_2O_5/TiO_2 for synthesis of phthalic anhydride

Bjoern Schimmoeller^a, Heiko Schulz^a, Sotiris E. Pratsinis^{a,*}, Anika Bareiss^b, Andreas Reitzmann^b, Bettina Kraushaar-Czarnetzki^b

^a Particle Technology Laboratory, Institute of Process Engineering, Department of Mechanical and Process Engineering, ETH Zurich, CH-8092 Zurich, Switzerland

^b Institute of Chemical Process Engineering, Department of Chemical Engineering and Process Engineering, University of Karlsruhe (TH), D-76128 Karlsruhe, Germany

Received 4 July 2006; accepted 9 July 2006

Available online 22 August 2006

Abstract

Flame-made airborne V_2O_5/TiO_2 nanoparticles were deposited directly onto mullite foam supports to create ready-to-use catalysts for the *o*-xylene conversion to phthalic anhydride. These particles containing 10% (w/w) V_2O_5 were created by combustion of liquid precursor sprays and characterized by transmission electron microscopy, nitrogen adsorption, X-ray diffraction (XRD), temperature-programmed reduction (TPR), and Raman spectroscopy. The specific surface area, anatase content, and dominantly monomeric vanadia species on titania were thermally stable up to 450 °C. Catalyst structure was controlled in situ during deposition by the particle-laden gas flow rate through the foam, resulting in homogeneous to patchy V_2O_5/TiO_2 coatings. The catalytic activity and selectivity were affected by both coating texture and particle morphology. These flame-coated foams showed superior catalytic activity and selectivity at high conversions than classic, wet-made V_2O_5/TiO_2 catalysts.

© 2006 Elsevier Inc. All rights reserved.

Keywords: Flame-spray pyrolysis; Direct deposition; Ceramic; Foam; Sponge; Partial oxidation; *o*-Xylene; Vanadia/titania; Raman spectroscopy

1. Introduction

The partial oxidation of *o*-xylene on V_2O_5/TiO_2 catalysts with O_2 from air in multiple parallel fixed-bed reactors is a highly exothermic reaction (1300–1800 kJ mol⁻¹) with a worldwide phthalic anhydride (PA) production of more than 3.7 million tons per year (1996) [1]. The PA is an important intermediate product in manufacture of commodity chemicals, such as modifiers for rubber and polymers. During its synthesis, evolving heat must be effectively transferred out of the catalyst bed, because hot spots above 500 °C irreversibly deactivate the catalyst [2], leading to increased risk of thermal reactor runaway. Usually for this reaction, “egg-shell” vanadia/titania catalysts of millimeter size with solid, inert cores are packed into a fixed bed. The thickness of the catalytically active shell is typically up to 100 μm [3]. This type of catalyst is used to prevent

activity and PA selectivity reduction by mass transfer limitations inside the porous catalyst. However, high pressure drop over low-porosity (40–45%) packed beds containing these catalyst pellets often limits PA productivity [4]. The pellet shape affects the catalyst bed porosity; thus, hollow cylinders or rings are commonly used to keep the pressure drop as low as possible [5].

An alternative approach is the application of ceramic foams as catalyst supports [6]. Such foams offer the possibility of improving reactor performance, especially for highly exothermic and fast chemical reactions, because heat transfer is enhanced compared with packed beds of spherical or cylindrical pellets [7]. The open-pore structure and the high void fraction (up to 95%) of ceramic foams lead to a lower pressure drop and increased heat transfer by radiation compared with packed beds [6]. In contrast to the laminar, separated flow in honeycombs, radial gas dispersion and higher gas turbulence is possible, increasing heat and mass transfer in the structure [6,8]. In addition, thermal conductivity and surface properties

* Corresponding author. Fax: +41 44 632 1595.
E-mail address: pratsinis@ptl.mavt.ethz.ch (S.E. Pratsinis).

of the support can be selected from a large variety of foam materials [9], so that foams can combine properties of packed beds and honeycombs [6,7]. Recently, the use of ceramic foam supports in the oxidation of *o*-xylene to PA was evaluated theoretically, showing that smooth axial and radial temperature gradients were less pronounced, reducing the risk of both reactor runaway and catalyst deactivation [10].

A high dispersion of vanadia on titania, enabling good accessibility of vanadia, is crucial for high activity. Monomeric and polymeric vanadia species showed enhanced reactivity in selective oxidations compared to crystalline vanadia [11]. Selectivity is mainly influenced by the vanadium oxidation state and its modifications during catalytic reaction [11]. However, the vanadia species that will result in highest activity and selectivity has not been identified yet [12] and might also depend on the reaction conditions [13]. Industrial V_2O_5/TiO_2 catalysts are very complex, containing several dopants like Cs and Sb that influence activity and selectivity to the desired product compared with the undoped catalyst [14,15].

Vanadia/titania catalysts have been made in vapor-fed flames ($4\text{--}200\text{ g h}^{-1}$), resulting in high anatase fractions ($>90\%$, w/w), containing 0–10% (w/w) V_2O_5 of high dispersion [16] and specific surface areas (SSAs) ranging from 23 to $120\text{ m}^2\text{ g}^{-1}$ [17]. Flame-made catalysts exhibited an open-pore structure that might facilitate mass transfer limited reactions compared with wet-made catalysts [18]. Flame-spray pyrolysis (FSP) in particular, is a versatile process for producing mixed-metal oxides of nanoscale size and a promising technique for catalyst production [18]. Very recently it has been shown that direct deposition of flame-made materials can lead to highly efficient sensors [19]. Extending this to catalysis by combining the two steps of particle production by FSP and direct particle deposition on catalytic support (e.g., foams) may shorten the catalyst synthesis chain, thereby reducing production costs. The direct deposition of airborne nanoparticles on ceramic foam supports may lead to a different pore size structures [20] and porosities [19] than obtained by standard multistep wet coating techniques. The open-pore structure may be retained, promoting gas penetration into the active layer. Such flame-deposited layers exhibit good adhesion and thermal contact to the support [21] and porosities of around 98% [19].

In the present study, ready-to-use catalysts were produced by direct deposition of FSP-made V_2O_5/TiO_2 nanoparticles on ceramic foam supports. The influence of particle SSA, coating morphology, and deposition time on catalyst performance was investigated. Catalytic activity and selectivity in FSP-made and wet-made catalysts were compared.

2. Experimental

2.1. Catalyst preparation

Xylene (Fluka, $>98.5\%$) and acetonitrile (Fluka, $>99.5\%$) solvents were mixed (11:5 by volume) with appropriate amounts of titanium tetraisopropoxide (TTIP, Aldrich, $>97\%$) and vanadium oxo-triisopropoxide (Strem Chemicals, $>98\%$), resulting in titanium metal concentrations ranging from 0.1

to 3.4 (without solvent) mol L^{-1} and a V_2O_5 content of 10% (w/w) in the powder product [22].

Vanadia/titania mixed oxides were synthesized by FSP in a laboratory-scale reactor [23], a concentric two-phase nozzle with a capillary (0.42 mm i.d.) through which the liquid precursor was fed by a syringe pump (Inotec, IER-560). Through the first annulus (inner/outer diameter 0.71/0.95 mm) 5 L min^{-1} of dispersion gas (O_2 , Pan Gas, 99.95%) was fed with a pressure drop of 1.5 bar. The resulting spray was ignited by a circular premixed flame (6 mm i.d., 10 μm slit width) of CH_4 (1.5 L min^{-1} , Pan Gas 99.5%) and O_2 (3.2 L min^{-1}). An additional O_2 sheath flow (5 L min^{-1}) for complete combustion of the precursor was supplied through a ring of sinter metal (11 mm i.d., 18 mm o.d.). All gas-flow rates were adjusted by calibrated mass-flow controllers (Bronkhorst). Powders were collected on glass microfiber filters (Whatman GF/D, 257 mm diameter) by a vacuum pump (Busch SV 1025 B). The production rates ranging from 2.6 to 89.6 g h^{-1} ($0.1\text{--}3.4\text{ mol L}^{-1}$ TTIP) were controlled by the liquid precursor metal concentration. For sinter stability experiments, FSP-made vanadia/titania was sintered at $300\text{--}900\text{ }^\circ\text{C}$ for 5 h (heating rate $5\text{ }^\circ\text{C min}^{-1}$) in air in an oven (Carbolite, CWF 1300).

To deposit the airborne vanadia/titania on the porous supports, ceramic foams were installed upstream of an enclosed microfiber filter unit for particle collection (Fig. 1). The foams were mounted in a cooled (H_2O , 69 mL min^{-1}) double-wall tube (i.d. 16 mm, annulus i.d./o.d. 18/26 mm, length 160 mm) about 300 mm above the nozzle. The ceramic foams (Vesuvius, mullite, $Al_6O_{13}Si_2$, 20 pores per inch [ppi]; porosity 0.78) were 15 mm in diameter and 50 mm in length. To avoid wall slip of gases and particles, foam supports were wrapped into glass fiber tape (Horst, GB25) before installation. To estimate the mass of deposited vanadia/titania, the weight of the uncoated and coated foam was measured (Mettler Toledo, AB204S). It should be noted that the foam weight did not change during installation and dismounting. All FSP-made catalysts were coated with 24–32 mg of V_2O_5/TiO_2 . The pressure drop over foam and filter was adjusted from 20 to 300 mbar with an exhaust throttle valve (MKS, Type 653 B) and a digital PID pressure controller (MKS, Type 651C, Baraton pressure transducer). The deposition time was 15–960 s.

For comparison, a 10% (w/w) vanadia/titania reference catalyst was also prepared by standard impregnation [24]. Vanadia (V_2O_5 , Fluka, $>99\%$) was dissolved in deionized water containing oxalic acid (molar ratio of V_2O_5 :oxalic acid = 1:4). An appropriate amount of titania (TiO_2 , anatase, Riedel-de-Haën, $9.1\text{ m}^2\text{ g}^{-1}$, 99.5–100% purity) was added to the solution. The suspension was mixed in a rotary evaporator for several hours, and water was evaporated. The material was dried at $65\text{ }^\circ\text{C}$ in air overnight, crushed (agglomerate size, 0.244–0.5 mm) and finally calcined (1 h, $450\text{ }^\circ\text{C}$, $1\text{ }^\circ\text{C min}^{-1}$) in air. Flame-made vanadia/titania was pelletized at 70 MPa, crushed, and sieved, with the same agglomerate size range as for the wet-made V_2O_5/TiO_2 . In what follows, these compacted catalysts and the wet-made catalysts are both referred to as pellet catalysts.

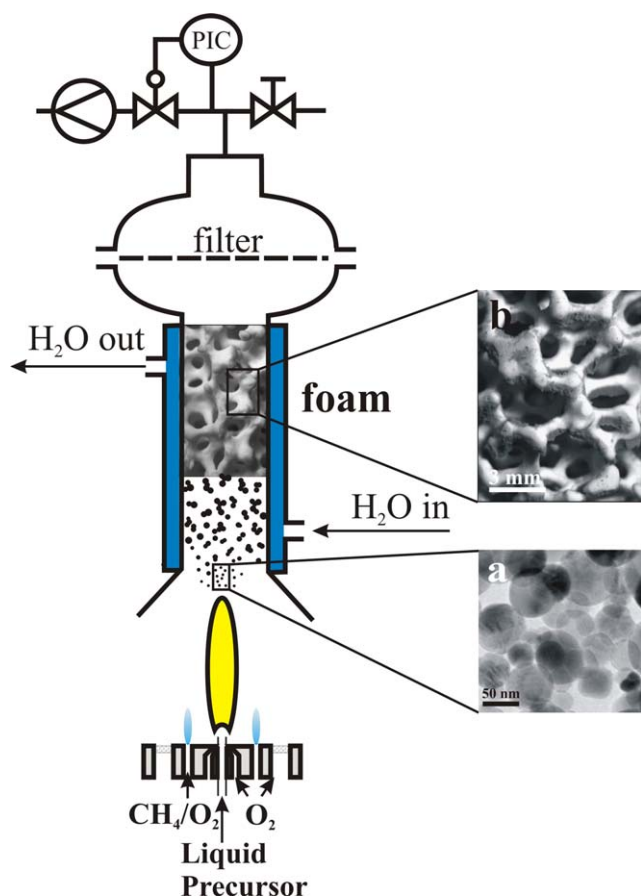


Fig. 1. FSP and foam deposition apparatus. V_2O_5/TiO_2 particle-laden gas flowed through the ceramic foam in the water-cooled deposition zone. Gas flows were controlled by the pressure drop over foam and filter resulting in homogeneous to patchy coatings. (a) shows a TEM image of the FSP-made particles ($53 \text{ m}^2 \text{ g}^{-1}$), (b) a coated ceramic foam with a patchy coating morphology.

2.2. Catalyst characterization

Powder SSAs (in $\text{m}^2 \text{ g}^{-1}$) were determined by nitrogen adsorption (Pan Gas, >99.999%) at 77 K by the Brunauer–Emmett–Teller (BET) method with a Micromeritics Tristar 3000 (five point-isotherm, $0.05 < p/p_0 < 0.25$). Assuming spherical, monodisperse primary particles with homogeneous density, the average BET particle diameter (d_{BET}) was calculated with 90% (w/w) titania (density anatase: $\rho = 3.8 \text{ g cm}^{-3}$; rutile: $\rho = 4.3 \text{ g cm}^{-3}$) and 10% (w/w) vanadia ($\rho = 3.4 \text{ g cm}^{-3}$). Before this analysis, the sample was heated (150°C , 1 h) with flowing N_2 (Pan Gas, >99.999%) to remove any adsorbed water. Pore size distributions were determined from desorption isotherms (Micromeritics ASAP 2010 Multigas system) using the Barrett–Joyner–Halenda (BJH) method [25]. Before this analysis, the sample was heated (200°C for more than 3 h) under vacuum to remove any adsorbed water. Monolayer coverage was calculated by assuming $10 \text{ V-atoms nm}^{-2}$ corresponding to one monolayer [26].

X-ray diffraction (XRD) was performed on a Bruker D8 Advance diffractometer (step size of 0.03° , scan speed of $0.60^\circ \text{ min}^{-1}$, $\text{CuK}\alpha$ radiation). Weight contents and crystal

sizes of titania were obtained by Topas 2.0 (model AXS 2000, Bruker) using the fundamental parameter approach and the Rietveld method [27]. Patterns were fitted for $2\theta = 19^\circ$ to 33° for anatase (ICSD #9853 [28]), rutile (ICSD #82656 [29]) and vanadia (ICSD #24042 [30]).

Temperature-programmed reduction (TPR) was used for the determination of average oxidation state (AOS) and reducibility analysis of vanadia. Experiments were carried out on a Micromeritics Autochem II 2920 unit equipped with a thermal conductivity detector by flowing 5 vol% H_2 in Ar (Pan Gas, >99.999%, 20 mL min^{-1}) through the sample. The temperature was increased from 50 to 950°C at a rate of $10^\circ\text{C min}^{-1}$. Before this analysis, the sample was oxidized in flowing oxygen (PanGas, >99.999%, 20 mL min^{-1} , 300°C , 30 min) to ensure complete oxidation of vanadia (+5). The total area under the peaks of the reduction spectra corresponds to the total amount of hydrogen consumed in the reduction process. Knowing the sample mass and vanadia content, the average oxidation state of the reduced material after TPR can be determined [31]. The highly oxidic conditions in the flame commonly result in complete oxidation of the reactants [32].

Raman spectroscopy was performed with a Renishaw InVia Reflex Raman system equipped with a 785-nm diode (solid state, 300 mW) laser as excitation source focused in a microscope (Leica, magnification $\times 50$). Three spectra were recorded (for 30 s) on a CCD camera after diffraction ($1200 \text{ lines mm}^{-1}$) using 0.3 mW of laser energy to avoid thermal alteration [33].

For transmission electron microscopy (TEM), materials were deposited onto a carbon foil supported by a copper grid. TEM analysis was performed with a CM30ST microscope (Philips; LaB6 cathode, operated at 300 kV, point resolution $\sim 2 \text{ \AA}$). SEM analysis was carried out on a Leo 1530 Gemini microscope (Zeiss, operated at a 2-kV field emission gun).

Catalyst effectiveness was estimated for pellets using the Weisz number ($\Psi = \ell^2 k_{\text{eff}} D_{\text{eff}}^{-1}$) and assuming first-order reaction kinetics for the rate of *o*-xylene consumption. The necessary parameters are given in Table 3. Average characteristic lengths were defined by assuming equal-sized spherical particles ($V_p A_p^{-1}$).

2.3. Catalytic testing

The partial oxidation of *o*-xylene was performed in an isothermal, laboratory-scale, fixed-bed reactor with plug flow behavior at 367°C . The reactor consisted of a vertically installed stainless steel tube (16 mm i.d., 380 mm long) that was electrically heated. The reactor and parts of the feed pipes were housed in an electrically heated (260°C) isolated box ensuring isothermal conditions throughout the reaction zone and preventing reactant condensation. All gases (N_2 , Air Liquide, >99.996%; O_2 , Air Liquide, >99.95%) and liquid *o*-xylene (Fluka, >99.0%) were fed by thermal mass-flow controllers (Bronkhorst). *o*-Xylene was evaporated with nitrogen at 100°C in an evaporator filled with inert material. Pressure in the reactor was adjusted to 1.3 bar. The molar fraction of *o*-xylene and oxygen in the reactor feed were 0.005 and 0.2, respectively. Total gas-flows ranged from 120 to 600 mL min^{-1} at stan-

standard conditions. Modified residence times (τ_{mod} , $\text{g}_{\text{cat}} \text{ s cm}^{-3}$) were defined as mass vanadia/titania in the reactor divided by the total gas flow under reaction conditions (367 °C, 1.3 bar). A controlled ethane flow (Air Liquide, 19.6 vol%, >99.5% in N_2 , >99.999%) was used as an internal standard for gas chromatography.

The fixed bed consists of three zones separated by glass wool to prevent SiC entrainment:

- (1) Initial break-in zone (length \approx 120–160 mm) consisting of either SiC particles (particle size, 1 mm) for the tests of the pellet catalysts or SiC particles and uncoated foam for the test of the foam catalysts.
- (2) Catalyst zone (length \approx 50–100 mm), pellets, wet-made (661 mg) or FSP-made pellet catalyst (45 mg) or a coated ceramic foam catalyst, wrapped with glass fiber tape to avoid wall effects (length 50 mm). Foams coated with $\text{V}_2\text{O}_5/\text{TiO}_2$ were in the same orientation with respect to gas flow direction as the FSP-coated foams. For the wet-made reference and FSP-made pellet catalyst measurements, the reactor was equipped with a thermo well (1 mm i.d.) located at the radial center of the reactor tube. A thermocouple inserted in the thermowell measured the temperature along the catalyst bed.
- (3) SiC particles (1 mm) to fill the remaining reactor volume (length \approx 100–160 mm).

3. Results

3.1. Characterization of $\text{V}_2\text{O}_5/\text{TiO}_2$

Pore size distributions of wet-made and flame-made particles and pellets are shown in Fig. 2a. Increasing the production rate from 17.6 to 89.6 g h^{-1} has no significant influence on the pore size distribution of flame-made $\text{V}_2\text{O}_5/\text{TiO}_2$. Most pores ranged from 20 to 100 nm (Fig. 2a, bottom) as ob-

served for FSP-made $\text{Ce}_{0.5}\text{Zr}_{0.5}\text{O}_2$ [34] and $\text{Pt}/\text{Al}_2\text{O}_3$ [18] particles. Pressing FSP-made particles into pellets changed SSA insignificantly and reduced pores sizes to 10–30 nm, further indicating that their porosity stems from the particle structure rather than particle pores [18]. The lower TEM image (Fig. 2c) shows flame-made $\text{V}_2\text{O}_5/\text{TiO}_2$ (17.6 g h^{-1}), corroborating the open pore structure of the material. No micrometer size particles were found by TEM analysis, indicating a homogeneous particle size distribution. The electron diffraction pattern (Fig. 2c, inset) shows the crystalline structure of these particles. The TEM image of calcined wet-made particles (Fig. 2b) shows nonspherical, nonporous vanadia/titania particles with sizes mainly >100 nm. The pore sizes of the corresponding pellet fraction ranged from 20 to 100 nm (Fig. 2a).

Fig. 3a compares TPR signal intensities from as-prepared FSP-made and calcined wet-made $\text{V}_2\text{O}_5/\text{TiO}_2$. The FSP-made powders showed one distinct reduction peak with a maximum intensity (T_{max}) at 483 °C, as observed for vapor-fed flame made $\text{V}_2\text{O}_5/\text{TiO}_2$ [16]. The wet-made material exhibited two distinct peaks at 546 and 694 °C, indicating reduction in several steps [35]. During reduction, the consumed H_2 was comparable for all samples, and thus the calculated average oxidation state (AOS) is nearly the same for all (Table 1). The influence of the sinter temperature on T_{max} of the FSP-made powder is shown in Fig. 3b (left axis). Sintering FSP-made particles up to 650 °C resulted in a shift of the maximum TPR signal (T_{max}) to higher temperatures, still with one distinct peak. Vanadia on titania is stable up to sintering temperatures of 450 °C, resulting in a constant T_{max} (triangles). With increasing sintering temperature up to 700 °C, the T_{max} increased up to 636 °C. The SSA of FSP-made $\text{V}_2\text{O}_5/\text{TiO}_2$ (squares, right axis) remained constant up to 450 °C as well. Increasing the sintering temperature from 450 to 900 °C resulted in a steep decrease of the SSA from 83 to 0.5 $\text{m}^2 \text{g}^{-1}$.

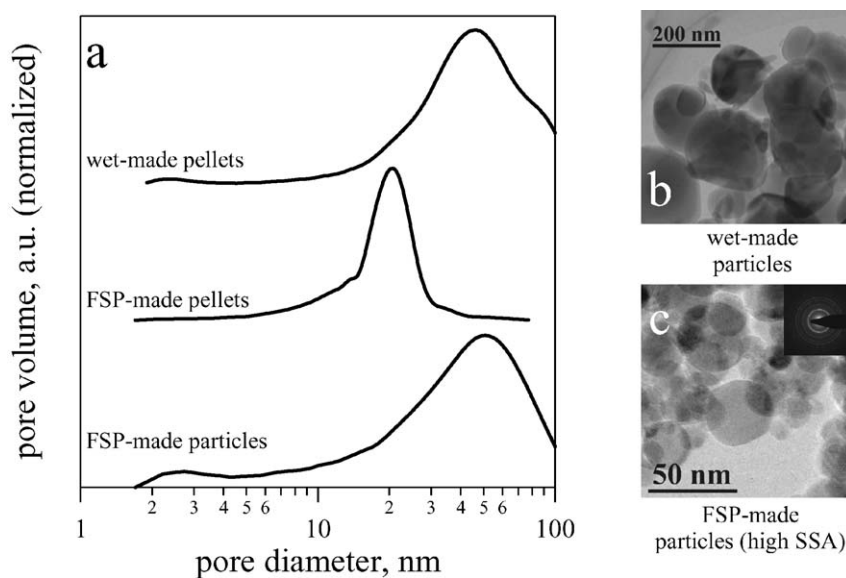


Fig. 2. (a) Pore size distributions of vanadia/titania from FSP-made particles are compared to FSP-made pellets and wet-made pellets. TEM images and electron diffraction patterns of the calcined wet-made (b) and flame-made (c) vanadia/titania show crystalline, solid nanoparticles.

The SSA of the powders decreased from 195 ($d_{\text{BET}} = 8$ nm) to 53 $\text{m}^2 \text{g}^{-1}$ ($d_{\text{BET}} = 29$ nm) with increasing $\text{V}_2\text{O}_5/\text{TiO}_2$ production rate (not shown) from 2.6 up to 89.6 g h^{-1} , as observed for vapor-fed flame-made $\text{V}_2\text{O}_5/\text{TiO}_2$ [17] and liquid-fed flame-made materials in general. Increasing particle-precursor concentration in the flame favors particle coagulation and coalescence, reducing the overall SSA [36]. The calcined wet-made reference sample had an SSA of 9 $\text{m}^2 \text{g}^{-1}$ ($d_{\text{BET}} = 200$ nm), smaller than all FSP-made powders (Table 1). Particles with 93 $\text{m}^2 \text{g}^{-1}$ were used for FSP-made pellets, retaining their SSA after pressing during pellet preparation.

For 10% (w/w) vanadia and titania not forming any interstitial solutions, the monolayer coverage was calculated from the SSA. For the FSP-made materials, the monolayer coverage ranged from 0.3 (195 $\text{m}^2 \text{g}^{-1}$) to 1.2 (53 $\text{m}^2 \text{g}^{-1}$), whereas the wet-made $\text{V}_2\text{O}_5/\text{TiO}_2$ had a coverage of 7.4 from its lower SSA (9 $\text{m}^2 \text{g}^{-1}$). The XRD pattern (not shown) of as-prepared

FSP-made vanadia/titania showed a high anatase crystal phase content (>94%, w/w) with no vanadia crystal structure consistent with vapor-fed flame-made $\text{V}_2\text{O}_5/\text{TiO}_2$ [16]. Broadening of peaks indicated anatase nanosized crystals of 17 to 29 nm (Table 1). The anatase size increased with increasing production rate from 10 up to 29 nm, having the lowest anatase content of 82% (w/w) at a production rate of 2.6 g h^{-1} and anatase content >94% (w/w) for production rates above 17.6 g h^{-1} $\text{V}_2\text{O}_5/\text{TiO}_2$. In contrast, the calcined, wet-made catalyst showed peaks of 6.8% (w/w) crystalline vanadia with a crystal size of 34 nm.

Fig. 4 shows Raman spectra of as-prepared 93 $\text{m}^2 \text{g}^{-1}$ and sintered FSP-made and wet-made calcined vanadia/titania. Spectra from the as-prepared and sintered (up to 450 °C) FSP-made powders exhibited a shoulder starting at a wavelength of 1033 cm^{-1} that corresponds to monomeric vanadium species [37]. Peak maxima at about 1005 cm^{-1} deviated slightly from Raman shifts of monomeric vanadia reported in the literature (1033 cm^{-1}), possibly due to partially hydrated $\text{V}=\text{O}$ bonds that shift the Raman bands to lower wavelengths [38,39]. With increasing sinter temperatures (above 500 °C), the shoulder intensity decreases and bands at 708 and 994 cm^{-1} appear, indicating the formation of crystalline vanadia [40]. A phase transformation of anatase crystals (638 cm^{-1}) into ru-

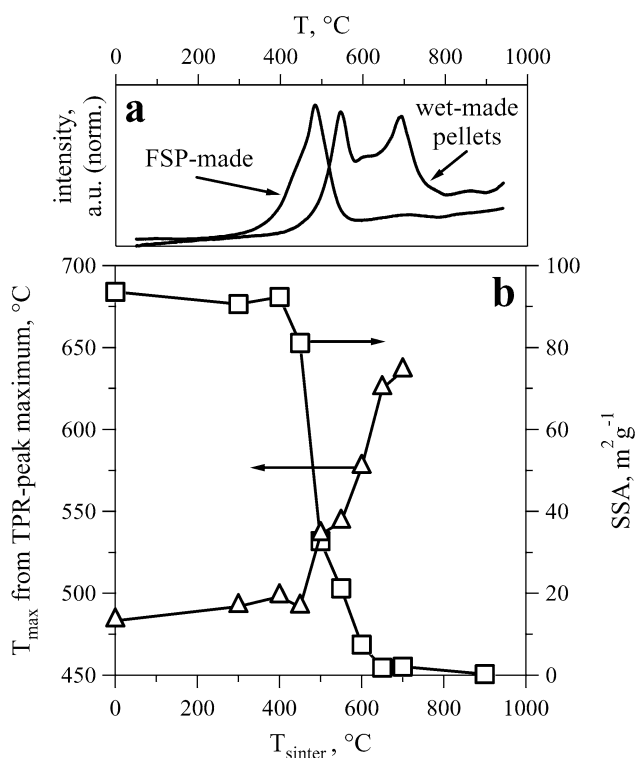


Fig. 3. (a) Temperature programmed reduction (TPR) analysis from as-prepared FSP-made and calcined wet-made (450 °C, 1 h) catalysts. The FSP-made $\text{V}_2\text{O}_5/\text{TiO}_2$ is reduced more easily than wet-made pellets. (b) The effect of sinter temperature on TPR peak maximum (left) and SSA (right). The increase in T_{max} corresponds to the SSA reduction for sinter temperatures between 450 and 700 °C.

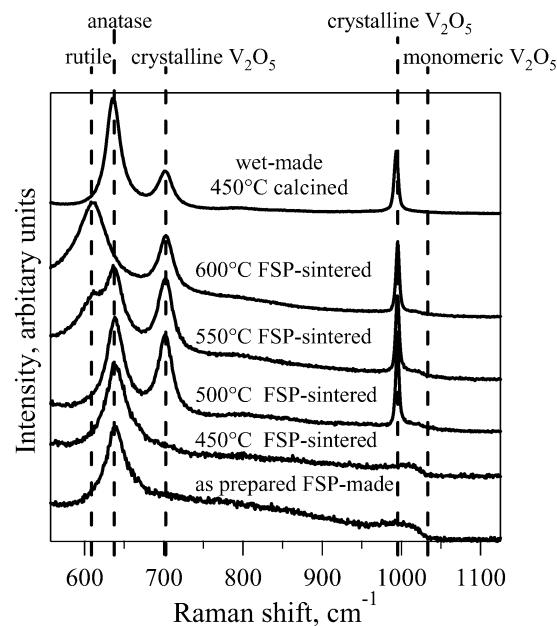


Fig. 4. Raman spectra of as-prepared and sintered FSP-made particles are compared to the wet-made calcined (450 °C) vanadia/titania particles. Flame-made powders are stable up to 450 °C. Above that, 450 °C crystalline vanadia structures were formed and between 500 and 600 °C anatase transforms into rutile.

Table 1

BET, XRD and TPR results for 10% (w/w) vanadia/titania powders from different production conditions and the wet-made reference

Vanadia/titania	Production rate (g h^{-1})	SSA ($\text{m}^2 \text{g}^{-1}$)	d_{BET} (nm)	Anatase (% w/w)	Anatase size (nm)	Monolayer coverage	T_{max} (°C)	AOS
FSP-made pellets	17.2	85	19	>94	17	0.7	483	3.6
High-SSA particles	17.2	93	17	>94	17	0.7	483	3.5
Low-SSA particles	87.2	53	29	>98	32	1.2	520	3.6
Wet-made pellets	–	9	200	>93	144	7.4	546, 694	3.6

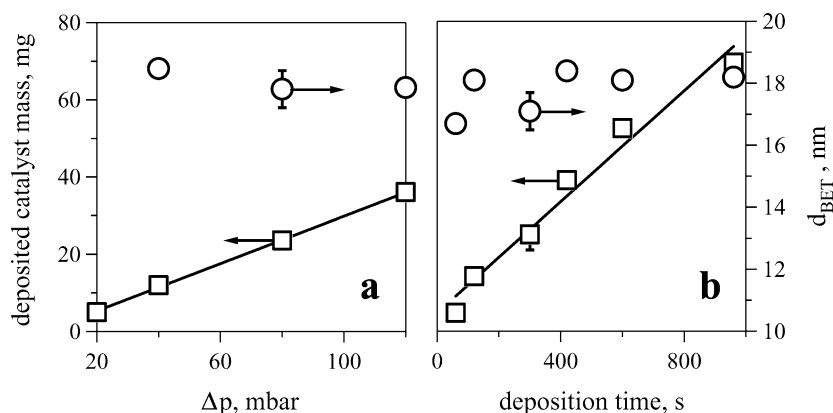


Fig. 5. The mass (squares) and average BET diameter d_{BET} (circles) of deposited vanadia/titania as a function of (a) pressure drop over foam and filter for a constant deposition time of 300 s and (b) deposition time for a constant pressure drop of 80 mbar. The d_{BET} did not change significantly at various deposition conditions indicating the stability of particle production by FSP during deposition over long periods.

tile crystals (608 cm^{-1}) above 500°C could also be observed; the peak intensity corresponding to anatase decreased, whereas the peak intensity corresponding to rutile increased. After sintering at 600°C , only rutile was detected, which corresponded to XRD results (not shown). Raman spectra of the FSP-made vanadia/titania with low SSA ($53 \text{ m}^2 \text{ g}^{-1}$, not shown) exhibited both a band at 1033 cm^{-1} and a weak and broad Raman band at $800\text{--}900 \text{ cm}^{-1}$ corresponding to polymeric vanadates [41]. Wet-made $\text{V}_2\text{O}_5/\text{TiO}_2$ (calcined at 450°C) showed only crystalline vanadia bands and Raman shifts corresponding to anatase [24], corroborating the XRD results.

3.2. Direct deposition of catalyst onto mullite foam

Vanadia/titania particles from two different FSP production conditions with 93 and $53 \text{ m}^2 \text{ g}^{-1}$ SSA (Table 1) were directly deposited onto mullite foams. With varying pressure drop across the foam and filter from 20 to 120 mbar at constant deposition time (300 s, Fig. 5a), the obtained coatings with high-SSA powder ($93 \text{ m}^2 \text{ g}^{-1}$) were nearly homogeneous (Fig. 6b). The deposited vanadia/titania mass was in the range of 5–25 mg. Increasing the pressure drop across foam and filter at a constant deposition time resulted in a linear increase of deposited $\text{V}_2\text{O}_5/\text{TiO}_2$ mass without significantly changing the homogeneous coating morphology. For depositing higher catalyst mass (25–70 mg), pressure drop was kept constant (80 mbar, Fig. 5b) and deposition time was increased to retain the homogeneous coating morphology. Increasing the deposition time up to 960 s 80 mbar, linearly increased the deposited mass also. The d_{BET} (circles) of the powder did not change significantly with changing deposition conditions, indicating the stability of particle production by FSP during deposition over long periods. Higher pressure drops ($\Delta p \geq 200$ mbar) resulted in more patchy coatings (Fig. 6c).

Fig. 6 shows images of uncoated (a), nearly homogeneous (b), and a patchy (c) $\text{V}_2\text{O}_5/\text{TiO}_2$ ($93 \text{ m}^2 \text{ g}^{-1}$) coatings of the foam support. Arrows indicate the particle-laden gas-flow direction during deposition. Coating thicknesses were in the sub-millimeter range, as shown in the SEM image (Fig. 6d) of

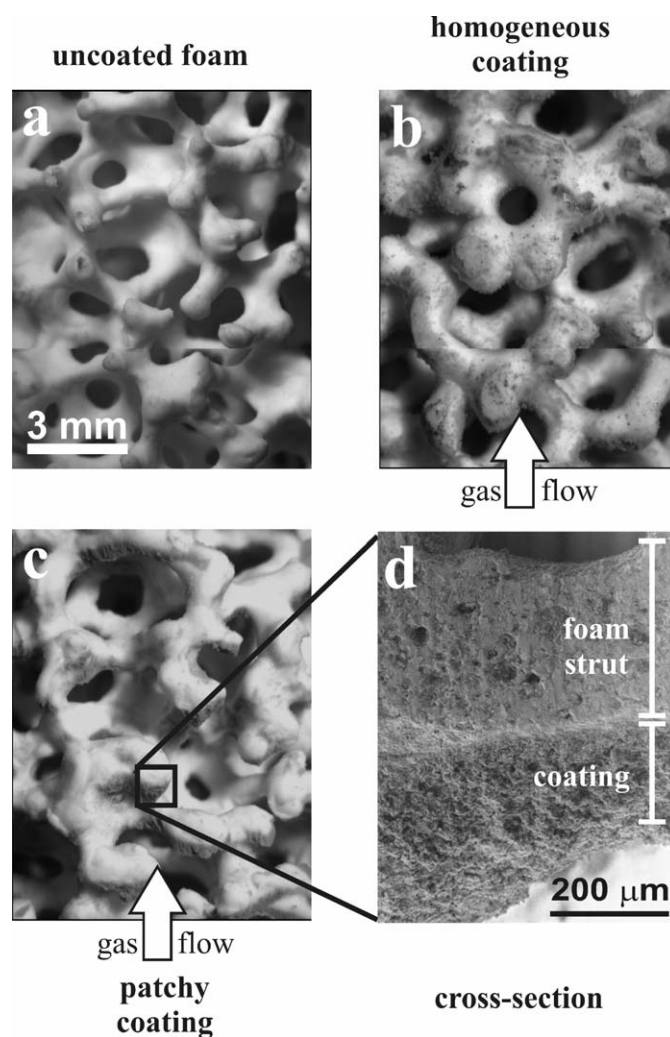


Fig. 6. Influence of coating conditions on the foam coating morphology in comparison to an (a) uncoated foam. Homogeneous coatings (b) were achieved by a low and constant pressure drop (80 mbar) over foam and filter (deposited catalyst mass = 25 mg). Patchy coatings (c, d) were achieved by pressure drop between 200 and 300 mbar (deposited catalyst mass = 38 mg).

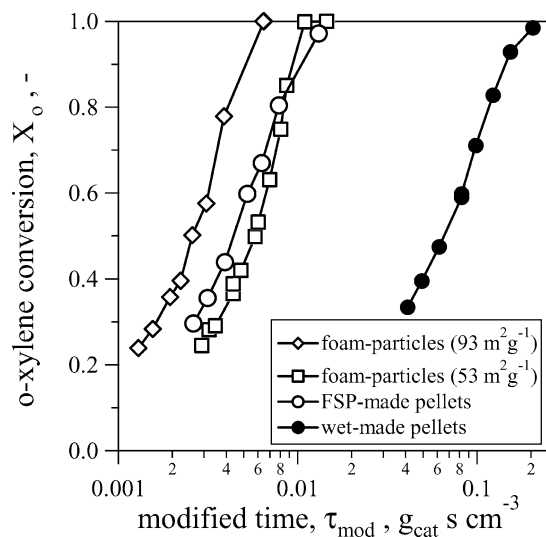


Fig. 7. Conversion of *o*-xylene as a function of the modified residence time τ_{mod} FSP-coated foam catalysts with high ($93 \text{ m}^2 \text{ g}^{-1}$, diamonds) and low ($53 \text{ m}^2 \text{ g}^{-1}$, squares) SSA particles, FSP-made high SSA particle pellets (open circles) and wet-made particle pellets (filled circles). FSP-made catalysts showed significantly higher activity than the wet-made reference.

a cross-section of a coated foam strut. Depositing 50 mg of $\text{V}_2\text{O}_5/\text{TiO}_2$ resulted up to 300- μm -thick layers.

3.3. Catalytic performance

The period of catalytic testing was 20–25 h for each catalyst. For a given *o*-xylene conversion, all data were measured over a 2-h period, taking on-line samples every 15 min. After measuring at full conversion, a point at lower conversion was measured again. No indication of changes in catalytic behavior during the time on stream was observed, consistent with literature reports for anatase [42] indicating the stability of flame-made catalysts. The constant catalytic performance during time on stream also indicates rather strong adhesion of $\text{V}_2\text{O}_5/\text{TiO}_2$ particle coatings on ceramic foams. Fig. 7 shows the *o*-xylene conversion as a function of modified residence time scaled by total gas flow and catalyst mass ($\text{g}_{\text{cat}} \text{ s cm}^{-3}$) of foams with homogeneous coatings by low (squares) and high (diamonds) SSA FSP-made $\text{V}_2\text{O}_5/\text{TiO}_2$, pellets with high SSA FSP-made particle (open circles) and wet-made pellets (filled circles) as reference. The catalysts are compared on a mass basis as has been done for selective reduction of *o*-xylene [3, 43] and oxidative dehydrogenation of propane [44], because the determination of catalyst volume for pellets was not unambiguous; the latter had been diluted with SiC to ensure isothermal conditions during testing for each *o*-xylene conversion. Coated foams with high SSA $\text{V}_2\text{O}_5/\text{TiO}_2$ showed the highest activity of all catalysts. Pellets of FSP-made catalysts reached full conversion after 0.004–0.02 g s cm^{-3} , faster than for wet-made pellets by at least one order of magnitude (0.2 g s cm^{-3}). Vanadia/titania with low SSA ($53 \text{ m}^2 \text{ g}^{-1}$) resulted in less active catalyst than powder with high SSA. Additional coated foam had to be installed in the catalytic reactor when testing the low-SSA $\text{V}_2\text{O}_5/\text{TiO}_2$ to obtain full conversion. No significant differences in catalytic activity were found for catalysts

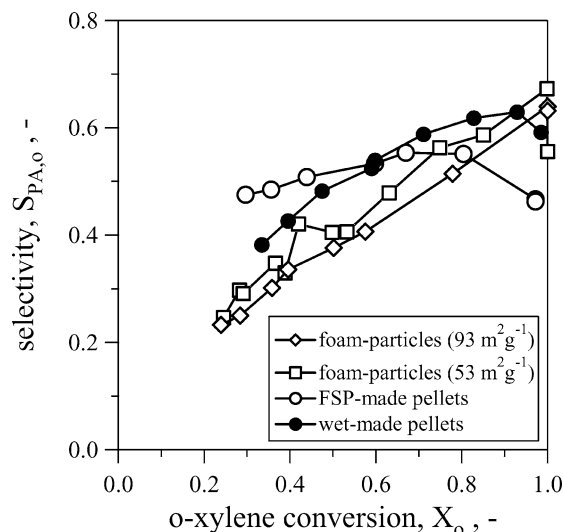


Fig. 8. Selectivity of phthalic anhydride as a function of *o*-xylene conversion for FSP-particle coated foam catalysts with high (diamonds) and low (squares) SSA particles, FSP-made pellets (open circles) and wet-made (filled circles) reference catalysts.

with homogeneous and patchy (not shown) coatings of low-SSA vanadia/titania. FSP-made pellets of high-SSA particles showed similar activity as the coated foams with low-SSA vanadia/titania.

Fig. 8 compares selectivities to phthalic anhydride (PA) by coated foam and pellet catalysts as a function of *o*-xylene conversion, X_o . The selectivity to PA passes through a maximum for all catalysts with increasing *o*-xylene conversion (equivalent to longer residence time). The position of the maximum depends on catalyst type (Fig. 8): >99.9% conversion for the foam catalysts (squares, diamonds), 65–80% conversion for the FSP-made pellets (open circles), and 92% for the wet-made pellets. After passing the maximum, the selectivity decreased following the reaction sequence in which PA is an intermediate and subsequently converted to CO_x , leading to a drastic PA selectivity reduction for the foam catalysts at $X_o = 1$ (Fig. 8, squares). At $X_o = 0.2$ –0.70, higher selectivity to PA was obtained for both wet-made (filled circles) and flame-made (open circles) pellets compared with coated foam catalysts with high-SSA (diamonds) and low-SSA (squares) FSP-made particles. The FSP-made pellet catalyst (open circles) showed higher selectivity at low conversion ($X_o = 0.3$ –0.5) than the wet-made catalysts, but lower selectivities at conversions above $X_o = 0.6$.

Higher conversions (>0.95) resulted in inferior selectivities of both pellets than the foam catalysts. Selectivities of homogeneous (Fig. 8, squares) and patchy (not shown, Table 2) coatings with low-SSA $\text{V}_2\text{O}_5/\text{TiO}_2$ show comparable results. Foams coated with high-SSA $\text{V}_2\text{O}_5/\text{TiO}_2$ particles always exhibited lower selectivities than those coated with low-SSA particles.

Fig. 9 shows the selectivities of intermediates phthalide (PT), *o*-tolualdehyde (TA), and byproduct maleic anhydride (MA). Comparison between the coated foam catalysts and the FSP-made and wet-made particle pellets shows significant differences only in the intermediate concentrations, whereas the MA selectivity is between 2 and 5% independent of cata-

Table 2
Conversion, modified residence time, selectivity, yield and productivity for FSP- and wet-made V_2O_5/TiO_2 catalysts

Catalyst	X_o (%)	τ_{mod} ($10^{-3} \text{ g}_{cat} \text{ s cm}^{-3}$)	$S_{PA,o}$ (%)	Y_{PA} (%)	P_{PA} ($\text{kg}_{PA} \text{ h}^{-1} \text{ kg}_{cat}^{-1}$)
Homogeneous coated foam with high SSA particles	99	6.5	64	64	7.1
Homogeneous coated foam with low SSA particles	99	10.9	67	67	4.5
Patchy coated foam with low SSA particles	99	11.8	68	67	4.1
FSP-made pellets	97	13.1	48	45	2.5
Wet-made pellets	98	205	60	58	0.2

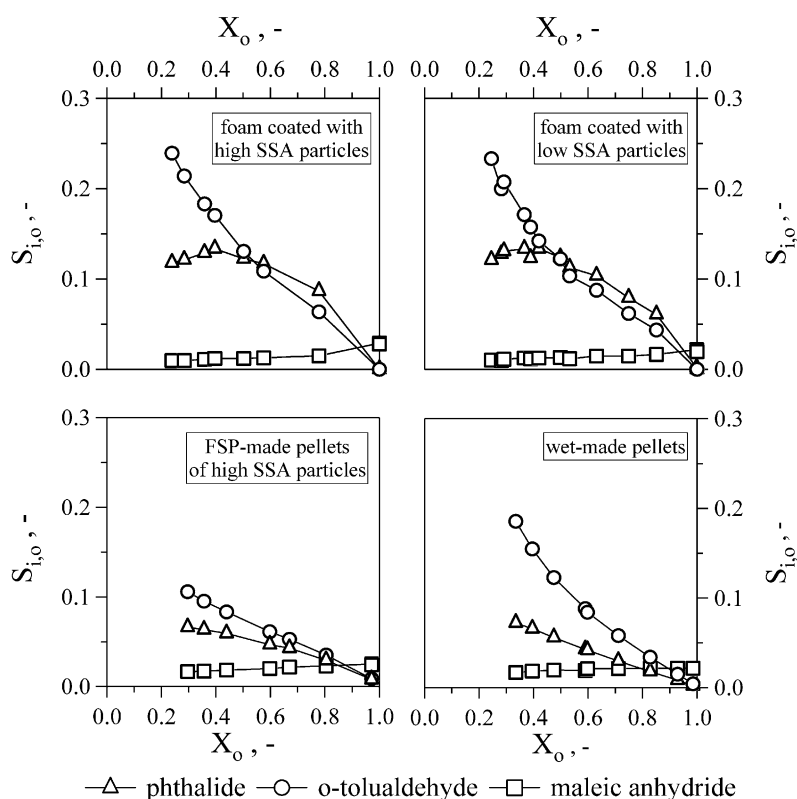


Fig. 9. Selectivity of intermediates phthalide (triangles), *o*-tolualdehyde (circles) and byproduct maleic anhydride (squares) as a function of *o*-xylene conversion for coated-foam catalysts with high and low SSA particles, FSP-made pellets and wet-made catalysts.

lyst. The selectivity to TA decreases for all catalysts with increasing conversion. At low conversions, it was significantly higher for catalysts containing FSP-made pellets and coated foams than for wet-made pellets. The SSA of particles coated on the foams did not influence the TA selectivity. The PT selectivity of foams was higher than for both of the pellets and reached a maximum before decreasing to very low values at high conversions. For high conversions, almost no PT or TA remained in product gas flow, resulting in MA as the main byproduct. However, the CO_2 selectivity (not shown) was rather stable (20–35%) at various *o*-xylene conversions and catalyst SSAs with no notable trend. For the FSP-made pellets, it reached up to 40% at full conversion. The CO selectivity was 3–10% for all catalysts over the entire *o*-xylene conversion range.

Table 2 compares conversion, residence time, selectivity, yield, and productivity for all tested catalysts at the highest selectivity at a given conversion. FSP-made V_2O_5/TiO_2 coated on mullite foams resulted in higher activities, selectivities, and yields than the wet-made catalyst. Stemming from the high catalytic activity, productivities of the coated foam catalysts were one order of magnitude higher than those of wet-made pellets.

4. Discussion

4.1. Particle characterization and deposition

Vanadia/titania nanoparticles with high anatase content (>94%, w/w) were made by FSP at high production rates ranging from 17.6 to 89.6 g h^{-1} . Having a significantly higher

Table 3
Weisz number and catalyst effectiveness of FSP- and wet-made pellet catalysts

Sample	Rate constant (1st order) ($\text{m}^3 \text{kg}_{\text{cat}}^{-1} \text{s}^{-1}$)	Eff. diffusion coefficient ($10^{-6} \text{m}^2 \text{s}^{-1}$)	Apparent cata- lyst density (kg m^{-3})	Av. character- istic length ^a (μm)	Pellet porosity (–)	Weisz number (–)	Catalyst effectiveness (–)
FSP-made pellets	0.181	1.15	1110	~60	0.43	1.09	0.67
Wet-made pellets	0.014	0.604	1620	~60	0.43	0.07	0.98

^a $V_p A_p^{-1}$, assuming equally sized spherical pellets.

SSA, flame-made $\text{V}_2\text{O}_5/\text{TiO}_2$ provided more external surface area than the wet-made material, resulting in monomeric vanadia species on the surface of the flame-made particles (Figs. 3 and 4). Peak TPR temperatures below 500°C indicate monomeric vanadia on titania, being reduced more easily than polymeric ($T_{\text{max}} \approx 540^\circ\text{C}$) or bulk ($T_{\text{max}} > 580^\circ\text{C}$) vanadia [11], leading to, in combination with the high SSA, superior catalytic activity of the FSP-made catalysts compared with the wet-made ones with crystalline vanadia (Fig. 7).

Sintering flame-made $\text{V}_2\text{O}_5/\text{TiO}_2$ for 5 h (5°C min^{-1}) did not change the titania composition or crystallinity up to 450°C . Starting at 500°C , the anatase began to transform into rutile; at 600°C , this phase change was completed [45]. The vanadia phase composition on TiO_2 did not change significantly for sintering temperatures up to 450°C (Figs. 3 and 4). The first vanadia crystal structures were detected above 500°C (not shown), corroborating the Raman results (Fig. 4). At higher sintering temperatures, the vanadia phase composition changed from dominantly monomeric to bulk vanadia (650°C) (Figs. 3 and 4). The dramatic decrease in SSA of the FSP-made vanadia/titania above 450°C (Fig. 3) corresponds to the anatase-to-rutile transformation (Fig. 4) and crystal growth.

The deposited $\text{V}_2\text{O}_5/\text{TiO}_2$ mass and coating morphology could be controlled in direct deposition (Figs. 5 and 6). At low gas flows through the foam (low pressure drop, <120 mbar), a nearly homogeneous coating over the foam was obtained (Fig. 6b). Under these conditions, the gas flow through the foam was rather slow, so that particles should be deposited mainly by diffusion and thermophoresis [19]. Increasing the gas flow through the foam (as measured by a greater pressure drop) resulted in more patchy, rather thick coatings (Figs. 6c and 6d). Under these conditions, deposition was caused mainly by impaction, because vanadia/titania is found mostly on foam locations facing the particle-laden gas flow.

Although the porosity of the layer on the foams was not determined here, results of direct deposition of FSP-made particles on flat surfaces by diffusion and thermophoresis [19] showed a high layer porosity of 98%. Pore sizes ranging from 10 to 100 nm in the deposited layer of the coating are assumed to be comparable to those in the nanoparticle beds (Fig. 2a: FSP-made high-SSA particles). Therefore, directly deposited FSP-made nanoparticles on mullite foams can facilitate the penetration of reactants into the catalytic layer by retaining the open pore structure compared with pelletized flame-made vanadia/titania (Fig. 2).

4.2. Catalytic testing

FSP-made vanadia/titania powder exhibited a broad pore size distribution with a maximum at 40–50 nm. During pelletizing of the FSP-made powder, particles were packed more closely, thereby reducing the average pore size to <20 nm (Fig. 2a). The FSP-made pellet catalyst showed slightly lower activity than the coated foams with high SSA (Fig. 7). Smaller pore sizes and longer diffusion times through the pellets may have led to inner mass transfer limitations, decreasing selectivity at high conversion and activity compared with coated foams and wet-made catalysts. *o*-Xylene reacts to phthalic anhydride inside the small pores of the catalyst pellets (Fig. 2a). PA trapped inside the pores is converted into high-oxidation products, CO and CO_2 . At low conversion, intermediates are cumulatively converted into PA due to possible mass transfer limitations, resulting in higher PA and lower phthalide and *o*-tolualdehyde selectivity compared with the coated foam catalysts (Figs. 8 and 9). Therefore, pelletizing of nanoparticle agglomerates resulted in decreased selectivity toward PA by possibly hindering reactant diffusion. This was corroborated by estimating the Weisz number and catalyst effectiveness (Table 3) of the pellets. The rate of *o*-xylene conversion is affected by internal mass transfer only for the FSP-made particle pellets ($\Psi \sim 1.1$, catalyst effectiveness = 0.67, Table 3). Such low catalyst effectiveness must also affect the product selectivities by enhancing on the one hand the formation of PA from the intermediates and on the other hand the conversion of PA to CO_x in the pore system of FSP-made pellets. The absence of mass transfer limitations for the wet-made particles pellets ($\Psi < 0.1$) [46] arises from the low rates of *o*-xylene consumption compared with the catalysts containing FSP-made particles.

For coated foam catalysts, no indications of inner mass transfer limitations were observed; instead, selectivity increased with increasing *o*-xylene conversion until selectivity collapsed at a conversion of 99+%. Maximum selectivities of homogeneous or patchy coated foams with high- or low-SSA particles were higher than those of the wet-made catalyst. Reducing the SSA of the $\text{V}_2\text{O}_5/\text{TiO}_2$ from 93 down to $53 \text{m}^2 \text{g}^{-1}$, and offering less monomeric vanadia but also polymeric vanadate sites resulted in a less active coated foam catalyst (Fig. 7, squares) with slightly higher maximum selectivity (Fig. 8) compared with the coated foam catalyst with high-SSA particles. This might indicate that foam catalysts coated with high-SSA (and highly active) particles did not exhibit the preferred vanadia composition for high PA selectivities.

A broader comparison to the literature is rather challenging. Despite the different reactor types, temperatures, pressures, and initial concentrations of *o*-xylene, the investigated catalysts either had a different vanadia loading [11,47] or were doped with several promoters [48] as used in the commercial synthesis of phthalic anhydride by vanadia/titania catalysts. However, selectivities >73% for undoped V₂O₅/TiO₂ systems have been not reported [49]. This is only slightly higher than the results presented here. In terms of calculated productivity, P_{PA} , the advantages of FSP-coated foams are quite clear (Table 2). In general, promoters like Cs and Sb can also be introduced by FSP, which is a topic for future study.

5. Conclusion

Titania-containing 10% (w/w) vanadia nanoparticles were produced in single step by FSP having a submonolayer, monomeric V₂O₅ on the titania surface. The SSA and vanadia composition were thermally stable up to 450 °C. For higher sintering temperatures, the SSA decreased drastically by TiO₂ phase transformation and grain growth.

The direct deposition of flame-made vanadia/titania on mulite foams was controlled by the pressure drop over the foam

and/or filter, resulting in patchy to nearly homogeneous coatings of V₂O₅/TiO₂ on the foam. The coated-foam catalyst had higher catalytic activity and selectivity to phthalic anhydride at high *o*-xylene conversion compared with a wet-made catalyst. The high vanadia distribution and its monomeric composition on the titania facilitated vanadia accessibility. Homogeneous/patchy coatings of V₂O₅/TiO₂ with low SSA showed slightly higher yield than the homogeneous coatings with high SSA but with lower space-time yield. Directly coated foam catalysts combine high accessibility and high catalytic yield with favorable support structures (low pressure drop, enhanced heat transfer) and fast production routes, making them attractive for catalytic reactions.

Acknowledgments

The authors thank Dr. Frank Krumeich (ETH Zürich) for the electron microscope analysis. This work was supported by ETH Research Grant TH-41 06-1.

Appendix A

Table A
List of abbreviations and symbols

Symbol	Unit	Definition	Description
AOS	–	$AOS = 3 \cdot \frac{H_2 \text{ consumption}}{V \text{ content}}$	Average oxidation state
A_p	m ²	$A_p = \pi \cdot d_p^2$	Particle geometric surface area
d_{BET}	nm	$d_{BET} = \frac{6}{SSA \cdot \rho}$	Average BET diameter
d_p	m	–	Pellet diameter
D_{eff}	m ² s ⁻¹	–	Effective diffusion coefficient
FSP	–	–	Flame spray pyrolysis
k_{eff}	m ³ kg _{cat} ⁻¹ s ⁻¹	1st order	Rate constant
ℓ	m	$\ell = V_p/A_p$	Average characteristic length
MA	–	–	Maleic acid
m_{cat}	g	–	Mass of vanadia/titania
n_i	mol	–	Amount of substance
O	–	–	<i>o</i> -Xylene
PA	–	–	Phthalic anhydride
P_{PA}	kg _{PA} h ⁻¹ kg _{cat} ⁻¹	$P_{PA} = \frac{Y_{PA} \cdot \dot{M} \cdot 60}{m_{cat}} \cdot n_{o,0}$	Productivity
PT	–	–	Phthalid
SEM	–	–	Scanning electron microscopy
$S_{i,o}$	–	$S_{i,o} = \frac{v_i}{v_o} \frac{\dot{n}_i}{(n_{o,0} - \dot{n}_o)}$	Selectivity of substance <i>i</i>
SSA	m ² g ⁻¹	–	Specific surface area
TA	–	–	<i>o</i> -Tolualdehyde
TEM	–	–	Transmission electron microscopy
T_{max}	°C	–	Temperature of max. TPR peak
TPR	–	–	Temperature programmed reduction
T_{sinter}	°C	–	Sinter temperature
TTIP	–	–	Titanium tetraisopropoxide
\dot{V}_{gas}	mL min ⁻¹	–	Total gas flow
V_p	m ³	$V_p = \frac{\pi}{6} \cdot d_p^3$	Pellet volume
X_o	–	$X_o = \frac{(n_{o,0} - \dot{n}_o)}{n_{o,0}}$	Conversion of <i>o</i> -xylene
XRD	–	–	X-ray diffraction
Y_{Pa}	–	$Y_{Pa} = X_o \cdot S_{PA,o}$	Yield of phthalic anhydride
Δp	mbar	–	Pressure drop over foam and filter
ρ	g cm ⁻³	–	Density
τ_{mod}	g _{cat} s cm ⁻³	$\tau_{mod} = \frac{m_{cat}}{V_{gas}} (367 \text{ °C}, 1 \text{ m}, 3 \text{ bar})$	Modified residence time
ν_I	–	–	Stoichiometry coefficient
Ψ	–	$\Psi = \ell^2 \cdot \frac{k_{eff}}{D_{eff}}$	Weisz number

References

- [1] P.M. Lorz, F.K. Towae, N. Bhargava, Ullmann's Encyclopedia of Industrial Chemistry, Wiley-VCH, Weinheim, 2003, <http://dx.doi.org/10.1002/14356007>.
- [2] A.I. Anastasov, Chem. Eng. Process. 42 (2003) 449–460.
- [3] A.I. Anastasov, Chem. Eng. Sci. 58 (2003) 89–98.
- [4] T. Boger, M. Menegola, Ind. Eng. Chem. Res. 44 (2005) 30–40.
- [5] K. Blechschmitt, DE2510994, to BASF AG, 1975.
- [6] M.V. Twigg, J.T. Richardson, Chem. Eng. Res. Des. 80 (2002) 183–189.
- [7] Y. Peng, J.T. Richardson, Appl. Catal. A 266 (2004) 235–244.
- [8] J.T. Richardson, Y. Peng, D. Remue, Appl. Catal. A 204 (2000) 19–32.
- [9] F.C. Buciuman, B. Kraushaar-Czarnetzki, Ind. Eng. Chem. Res. 42 (2003) 1863–1869.
- [10] A. Reitzmann, A. Bareiss, B. Kraushaar-Czarnetzki, Oil Gas Eur. Mag. 32 (2006) 94–98.
- [11] G. Centi, Appl. Catal. A 147 (1996) 267–298.
- [12] M. Calatayud, C. Minot, J. Phys. Chem. B 108 (2004) 15679–15685.
- [13] N.Y. Topsoe, M. Anstrom, J.A. Dumesic, Catal. Lett. 76 (2001) 11–20.
- [14] B. Grzybowska-Swierkosz, Top. Catal. 21 (2002) 35–46.
- [15] F. Cavani, C. Cortelli, A. Frattini, B. Panzacchi, V. Ravaglia, F. Trifiro, C. Fumagalli, R. Leanza, G. Mazzoni, Stud. Surf. Sci. Catal. 155 (2005) 153–165.
- [16] W.J. Stark, K. Wegner, S.E. Pratsinis, A. Baiker, J. Catal. 197 (2001) 182–191.
- [17] W.J. Stark, A. Baiker, S.E. Pratsinis, Part. Part. Syst. Char. 19 (2002) 306–311.
- [18] R. Strobel, W.J. Stark, L. Madler, S.E. Pratsinis, A. Baiker, J. Catal. 213 (2003) 296–304.
- [19] L. Mädler, A. Roessler, S.E. Pratsinis, T. Sahn, A. Gurlo, U. Weimar, Sens. Actuators B 141 (2006) 283–295.
- [20] T. Johannessen, J.R. Jenson, M. Mosleh, J. Johansen, U. Quaade, H. Livbjerg, Chem. Eng. Res. Des. 82 (2004) 1444–1452.
- [21] S. Thybo, S. Jensen, J. Johansen, T. Johannessen, O. Hansen, U.J. Quaade, J. Catal. 223 (2004) 271–277.
- [22] S. Storck, J. Zuehlke, S. Neto, F. Rosowski, WO2004EP05247 20040515, to BASF AG, 2004.
- [23] L. Mädler, H.K. Kammler, R. Mueller, S.E. Pratsinis, J. Aerosol Sci. 33 (2002) 369–389.
- [24] I.E. Wachs, S.S. Chan, R.Y. Saleh, J. Catal. 91 (1985) 366–369.
- [25] P.A. Webb, C. Orr, Analytical Methods in Fine Particle Technology, Micromeritics Instrument Corporation, Norcross, 1997.
- [26] I.E. Wachs, R.Y. Saleh, S.S. Chan, C.C. Chersich, Appl. Catal. 15 (1985) 339–352.
- [27] R.W. Cheary, A.A. Coelho, J. Appl. Crystallogr. 31 (1998) 851–861.
- [28] M. Horn, E.P. Meagher, C.F. Schwerdt, Z. Kristallogr. 136 (1972) 273–281.
- [29] I.E. Grey, C. Li, D.M. MacRae, L.A. Bursill, J. Solid State Chem. 127 (1996) 240–247.
- [30] A. Bystrom, K.A. Wilhelmi, O. Brotzen, Acta Chem. Scand. 4 (1950) 1119–1130.
- [31] G.C. Bond, S.F. Tahir, Appl. Catal. 71 (1991) 1–31.
- [32] R. Strobel, J.D. Grunwaldt, A. Camenzind, S.E. Pratsinis, A. Baiker, Catal. Lett. 104 (2005) 9–16.
- [33] C. Cristiani, P. Forzatti, G. Busca, J. Catal. 116 (1989) 586–589.
- [34] H. Schulz, W.J. Stark, M. Maciejewski, S.E. Pratsinis, A. Baiker, J. Mater. Chem. 13 (2003) 2979–2984.
- [35] Y.H. Kim, H.I. Lee, Bull. Korean Chem. Soc. 20 (1999) 1457–1463.
- [36] S.E. Pratsinis, W.H. Zhu, S. Vemury, Powder Technol. 86 (1996) 87–93.
- [37] D.A. Bulushev, L. Kiwi-Minsker, F. Rainone, A. Renken, J. Catal. 205 (2002) 115–122.
- [38] J.M. Jehng, G. Deo, B.M. Weckhuysen, I.E. Wachs, J. Mol. Catal. A 110 (1996) 41–54.
- [39] G. Ramis, C. Cristiani, P. Forzatti, G. Busca, J. Catal. 124 (1990) 574–576.
- [40] F. Roozeboom, M.C. Mittelmeijerhazeleger, J.A. Moulijn, J. Medema, V.H.J. Debeer, P.J. Gellings, J. Phys. Chem. 84 (1980) 2783–2791.
- [41] G.T. Went, S.T. Oyama, A.T. Bell, J. Phys. Chem. 94 (1990) 4240–4246.
- [42] G. Centi, E. Giamello, D. Pinelli, F. Trifiro, J. Catal. 130 (1991) 220–237.
- [43] J.N. Papageorgiou, M.C. Abello, G.F. Froment, Appl. Catal. A 120 (1994) 17–43.
- [44] K. Routray, K. Reddy, G. Deo, Appl. Catal. A 265 (2004) 103–113.
- [45] K.N.P. Kumar, K. Keizer, A.J. Burggraaf, T. Okubo, H. Nagamoto, S. Morooka, Nature 358 (1992) 48–51.
- [46] P.A. Weisz, Z. Phys. Chem. N. F. 11 (1957).
- [47] C.R. Dias, M.F. Portela, M.A. Banares, M. Galan-Fereres, M. Lopez-Granados, M.A. Pena, J.L.G. Fierro, Appl. Catal. A 224 (2002) 141–151.
- [48] S. Anniballi, F. Cavani, A. Guerrini, B. Panzacchi, F. Trifiro, C. Fumagalli, R. Leanza, G. Mazzoni, Catal. Today 78 (2003) 117–129.
- [49] B. Grzybowska-Swierkosz, Appl. Catal. A 157 (1997) 263–310.